Article
Vol. 25, No. 5, p. 715–729, October 2021
https://doi.org/10.1007/s12303-020-0058-z
pISSN 1226-4806 eISSN 1598-7477
Geosciences Journal GJ

CO_2 storage capacity of anthracite coal in deep burial depth conditions and its potential uncertainty analysis: a case study of the No. 3 coal seam in the Zhengzhuang Block in Qinshui Basin, China

Hongjie Xu[1]*, Shuxun Sang[2], Jingfen Yang[1], and Huihu Liu[1]

[1]School of Earth and Environment, Anhui University of Science and Technology, Huainan, Anhui 232001, China
[2]School of Resources and Geoscience, China University of Mining and Technology, Xuzhou, Jiangsu 221008, China

ABSTRACT: The storage of CO_2 in deep unminable coal seams can mitigate greenhouse gas emissions. However, CO_2 storage in deep anthracite coal is complex with some uncertainties in the estimation of CO_2 storage capacity. Based on isothermal adsorption experiments and gas solubility experiments under high temperature and pressure conditions, the total storage capacity of CO_2 in anthracite coal is discussed. The results show that the absolute adsorption amount is over 44 cm^3/g at temperatures of 318.15, 335.65, and 353.15 K as well as adsorption equilibrium pressures of 10 MPa. The storage capacity of adsorbed and free gas is 35–70 cm^3/g and 5–8 cm^3/g, respectively, within a depth range of 1000–2000 m. The soluble gas can be ignored for its low content between 0.22 cm^3/g and 0.28 cm^3/g with a proportion of less than 1%. The storage capacity of CO_2 may be estimated inaccurately because of the heterogeneity and uncertainty of the macroscopic geological conditions and coal reservoir parameters. Taking the No. 3 coal seam in Zhengzhuang block as an example, the storage priority area was divided into supercritical area and subcritical area with five sub-areas according to storage conditions, and the storage capacity was calculated, showing a relatively good storage potential.

Key words: CO_2 storage, anthracite coal, capacity estimation with uncertainty, coal seam, block-scale

Manuscript received February 28, 2020; Manuscript accepted August 27, 2020

1. INTRODUCTION

CO_2 to enhance coalbed methane recovery (CO_2-ECBM) can not only enhance CH_4 recovery but also realize the CO_2 storage in coal seams (De Silva et al., 2012; Liu et al., 2020b). Previous studies have shown that there were large capacities of CO_2 storage in coal seams in the world (Gale and Freund, 2010), countries (Liu et al., 2005), basins or regions (Bachu, 2007; Kronimus et al., 2008). In China, the deep coal reservoirs widely developed with considerable coal gas content in coal-bearing basins is a potential geological body for CO_2 storage (Wen et al., 2019; Xu et al., 2019; Liu et al., 2020b; Xu et al., 2020). However, CO_2 storage in deep anthracite reservoir faces many problems, such as adsorption capacity of anthracite coal for CO_2, neglected storage capacity of free gas and soluble gas with an increasing trend via burial depth.

Deep unminable coal seams have been estimated to provide the important geological storage volumes worldwide (Pan et al., 2013; Gale et al., 2015). Present evaluation methods for CO_2 storage capacity in coal beds can be applied to assess theoretical capacity, effective capacity, practical capacity, and matched capacity by using various technical (geological and engineering) cut-off limits (Bachu et al., 2007). However, regarding adsorbed gas as a primary storage state, previous adsorption behaviors mainly focused on the adsorption response of intermediate ranked bituminous coal or the adsorption of anthracite under non-high temperature and high pressure (Li et al., 2010; De Silva and Ranjith, 2014; Ramasamy et al., 2014; Zhang et al., 2015; Liu et al., 2019b) rather than high pressure and temperature conditions. Meanwhile, some researchers pointed out that the tested adsorption isotherms were complex (Krooss et al., 2002; Bae and Bhatia, 2006; Kim et al., 2011; Jinlong et al., 2018; Fang et al., 2019; Liu

*Corresponding author:
Hongjie Xu
School of Earth and Environment, Anhui University of Science and Technology, No. 168 Taifeng Ave., Huainan, Anhui 232001, China
Tel: +86-5546631022, E-mail: hjxu@aust.edu.cn

et al., 2019c). The adsorption and desorption energy of gas in the coal matrix can result in the swelling and shrinking of coal matrix, as well as change in the specific surface area and total pore volume of the pore fractures (Liu et al., 2018; Liu et al., 2019c; Du et al., 2020). Furthermore, the soluble gas content and free gas content are not concerned. But having water is a significant characteristic in coalbeds in China, and the free gas may be varying with the increasing of the coal depth.

But so far, the estimation method of CO_2 storage capacity in coal seams lacks sufficient accuracy for some simplifications or hypothesis. Also some geological parameters, such as coal heterogeneity and gas saturation of coal seams, coal gas content, coal bed thickness are still hard to consider (Bachu, 2007; Kronimus et al., 2008; Zhao et al., 2016). Especially, for anthracite reservoirs, CO_2 storage in deep burial depth conditions faces more problems and uncertainties, such as adsorption capacity of anthracite coal for CO_2, neglected storage capacity of free gas, and soluble gas with an increasing trend via burial depth. Further, the presence of water will also provide some additional storage capacity (through dissolution of CO_2) (Zhao et al., 2016). The water content has a dominant or even overriding effect on the gas storage capacity of coals (Busch and Gensterblum, 2011). Unfortunately, there is a lack of case studies in this area.

It is known that CO_2 reacts with minerals to get a storage capacity. However, the capacity of this part can be thought to be ignored as to the origin of the CO_2 coming from a transformation of adsorbed gas, free gas, or soluble gas with a long-term mineralization. Hence, the capacity of coal to store CO_2 allows adsorbed gas, free gas and soluble gas to be considered as primary states of storage that are required for any meaningful evaluation. Several papers (Sakurovs et al., 2009; Busch and Gensterblum, 2011; Höller and Viebahn, 2016; Ampomah et al., 2017; Chen et al., 2020; Tayari and Blumsack, 2020) provide external geological uncertainties in recording CO_2 storage capacity but do not compare the calculation parameters directly. Some calculated parameters, such as coal porosity, water saturation, and CO_2 compressibility factor also need to be considered. These parameters are all uncertain and difficult to obtain because of the heterogeneity of the coal reservoir.

This paper presents some fundamental considerations and observations, mainly based on laboratory experiments, to outline how the sorption capacity of deep anthracite coal (1000–2000 m), total CO_2 storage capacity (including free gas and soluble gas), and calculated uncertainty analysis through the study of anthracite coal samples collected from the deep No. 3 coal seam in collieries of the Southern Qinshui Basin, China.

2. GEOLOGICAL SETTING

Because the geological structures, hydrology, and coal seams in the Zhengzhuang block have been detailed in previous studies (Liu et al., 2014; Chen et al., 2018), only a brief summary of these characteristics is presented in this paper.

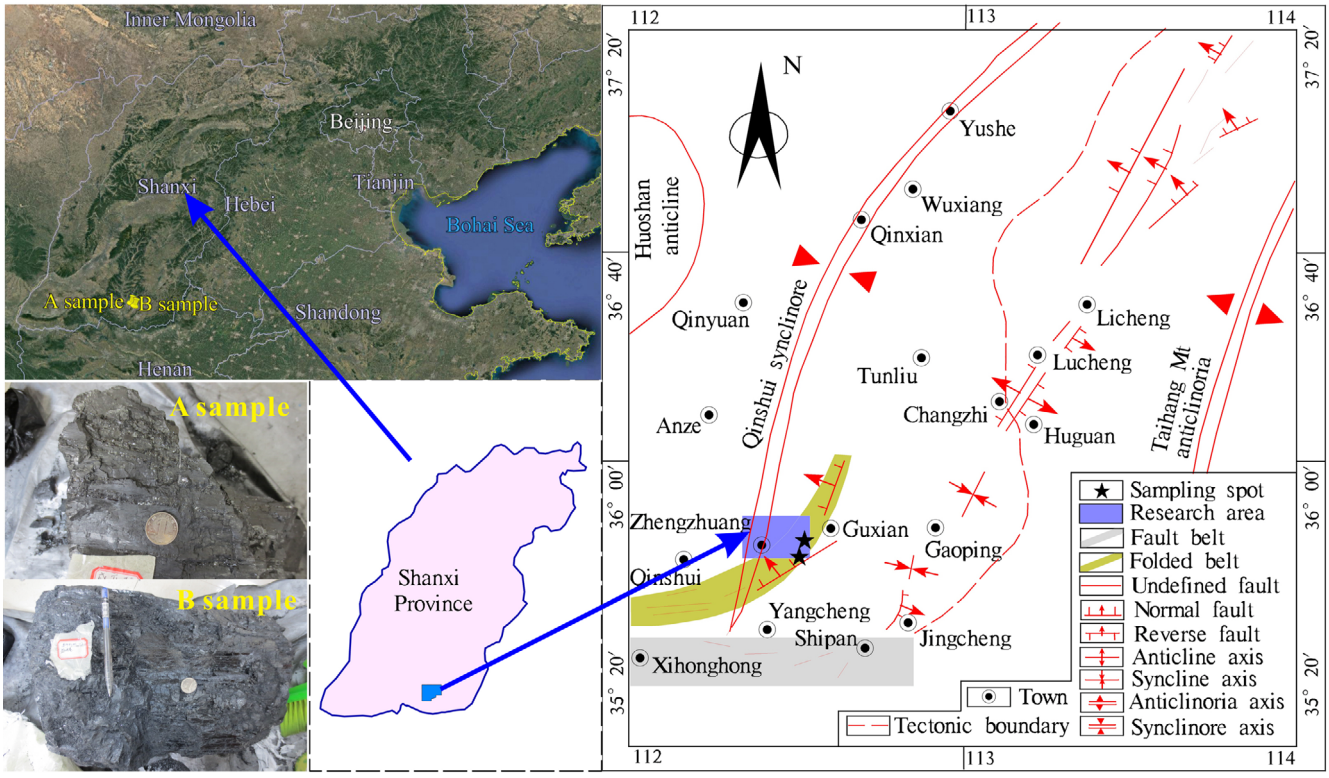

Fig. 1. Location of anthracite samples and structure outline of study area in China.

The Zhengzhuang block is located in the south of the Qinshui basin, north China (Fig. 1), which is the most important development area and first commercial exploitation area of coalbed methane (CBM) in China at present. The block belongs to the Jincheng administrative district of Shanxi Province, on the west side of the Fanzhuang block, bounded by the Sitou fault. The region comprises an area of more than 980 km^2 and is quite rich in CBM resources (Cai et al., 2011). Coal seams in the Zhengzhuang block are part of the Taiyuan Formation of the Upper Carboniferous and the Shanxi Formation of the Lower Permian. The primary coal seams containing CBM are the No.3 coal seam of the Shanxi Formation and the No. 15 coal seam of the Taiyuan Formation. The roof of No.3 coal seam is mainly mudstone and sandy mudstone mixed with minor siltstone and fine-grained sandstone; the floor is mainly mudstone and sandy mudstone and in some places, fine grain sandstone or siltstone. Compared with other domestic coal basins, the coals in the study area are typical high-rank coal reservoirs (R_o, 2.5–4.5%), while the gas content (10–37 cm^3/g) of the coal is also high in the Basin (Su et al., 2005). The No.3 coal seam is the main production layer for CBM because of its larger adsorption saturation (87%), critical desorption pressure (4.4 MPa), thickness (> 5.4 m), gas content (average 21.32 cm^3/g), and formation pressure (5.24 MPa) (Liu et al., 2013b).

3. MATERIALS AND METHODS

3.1. Samples and Preparation

Two typical coal samples were collected from large coal blocks from the Southern Qinshui Basin, Shanxi, China (Fig. 1). These two representative samples was selected to study the CO_2 storage in coal under high pressure and temperature conditions. They are all anthracite and defined as A and B. To prevent the samples from further oxidation, the collected bulk coal specimens were wrapped in plastic wrap and quickly packed, and immediately carried to laboratories. These samples were crushed and sieved to particles with different sizes for measurements. All the coal samples were tested with well-established measurement methods including measurements of the maceral, proximate, vitrinite reflectance, porosity, and minerals composition etc. Proximate, maceral composition, and specific surface analyses were conducted according to Chinese National standard GB/T 212-2008 (2008), GB/T 8899-2013 (2013) and GB/T 21650-2008 (2008). Although mercury intrusion porosimetry may give erroneous results for coal due to its flexibility, the obtained results of this method were considered to provide acceptable parameters in this paper. Mercury porosimetry analysis was carried out with the Auto-Pore IV 9500, using the mercury filling at pressures of up to 410 MPa permitting characterization of pore diameters exceeding 3.2 nm. Table 1 summaries the proximate, ultimate, maceral and mercury intrusion data for the selected coal samples.

3.2. Experimental Apparatus and Procedure

3.2.1. High-pressure sorption experiments

The schematic diagram of CO_2 adsorption experiment apparatus of DXF-II (Fig. 2), by the volumetric method according to Chinese National Standard GB/T 19560-2008 (2008). The experiment set up basically consists of a booster pump, a vacuum pump, a sample cell and reference cell with connected transducer. The system is able to withstand high pressures. A booster pump supplied CO_2 to the system at constant pressure. All cells and the associated tubing are held in a thermostatic water bath and maintained at a constant temperature to within ±1 K of the set point. All of pressures and temperatures were continuously

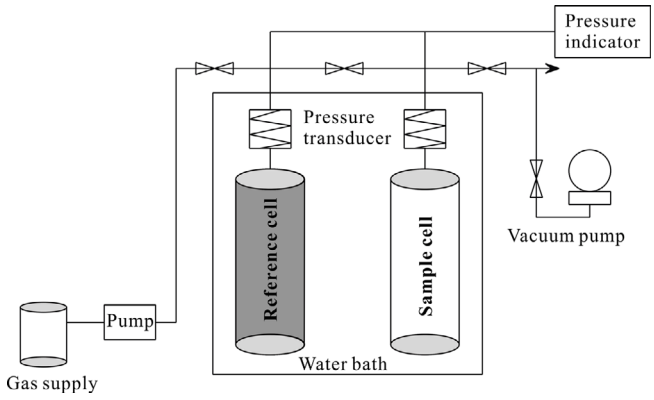

Fig. 2. Schematic diagram of high-pressure experimental apparatus of DXF-II for measuring CO_2/$ScCO_2$ adsorption.

Table 1. Properties of the selected coal samples

Samples	$R_{o,max}$ (%)	Proximate analysis (wt%)				Ultimate analysis (wt%)					Maceral composition (vol%)				Mercury intrusion		
		M_{ad}	A_{ad}	V_{daf}	F_{cad}	O_{daf}	C_{daf}	H_{daf}	N_{daf}	S_{daf}	Vit	Ine	Lip	Min	φ	ρ_{bulk}	$\rho_{skeletal}$
A	2.96	2.71	12.18	6.94	81.72	3.27	92.84	2.31	1.01	0.39	75.80	21.40	0	2.80	4.84	1.26	1.33
B	3.33	1.48	13.12	6.32	81.39	2.98	93.45	2.15	1.00	0.32	79.84	18.36	0	1.80	4.22	1.30	1.36

Note: M_{ad}, moisture content of air-dried basis; A_{ad}, ash content of air-dried basis; V_{daf}, volatile content of dry ash-free basis; F_{Cad}, fixed carbon carbon content of air-dried basis; O_{daf}, oxygen content of dry ash-free basis; C_{daf}, carbon content of dry ash-free basis; H_{daf}, hydrogen content of dry ash-free basis; N_{daf}, nitrogen content of dry ash-free basis; S_{daf}, Sulphur content of dry ash-free basis; Vit, vitrinite; Iip, liptinite; Exi, exinite; Min, mineral; ρ_{bulk}, bulk density, g/cm^3; $\rho_{skeletal}$, apparent (skeletal) density, g/cm^3.

https://doi.org/10.1007/s12303-020-0058-z

monitored with transducers. The accuracy and stability of these apparatus has been stated and some experimental results were previously reported in the corresponding research by Jinlong et al. (2018) and Liu et al. (2019b).

The A and B coal samples were initially reduced in size to 150 g (between 0.25 mm and 0.18 mm, to pass through a 60–80 mesh) and were equilibrated with moisture for at least 48 h prior to analysis as specified in the Standard Test Method for Equilibrium Moisture of Coal at 96–97 Percent Relative Humidity (ASTM D 1412-93). Prior to the start of the experiment, helium expansion was used to measure the void volume, which was defined as the total volume of helium that can penetrate in the sample cell with the sample inside. After that, the system completely evacuated and CO_2 dosed into the reference cell. As soon as the pressure equilibrium criteria were met (pressure variation less than 0.001 MPa in one minute or waiting for 30 minutes after dosing the gas into the reference cell), the valve between the two cells was opened, and the gas was injected into the sample cell.

In order to study CO_2 adsorption capacity as a function of depth (> 1000 m) with high pressure and temperature, the two samples selected for adsorption measurement were put in the instrument at three different temperatures (318.15, 335.65, and 353.15 K). These temperatures were considered relevant to coal seam depths (1000, 1500, 2000 m) with corresponding pressures of 10 MPa, 15 MPa and 20 MPa, respectively.

3.2.2. Solubility experiments

In order to determine the soluble gas content of coal, the solubility of CO_2 in coal seam water needs to be investigated. But only the deionized purified water samples were tested regretfully in this study. Nevertheless, the data tested by purified water were considered as an acceptable approach to determine the soluble gas content in coal. The CO_2 solubility analysis work was also carried out by the CO_2 adsorption experiment apparatus. The apparatus included in the system (Fig. 2) consists of the reference cell and sample as high pressure equilibrium cell and constant pressure cell, respectively. The equilibrium cell and its loading lines were evacuated down to 0.1 Pa and one liter of deionized purified water was added into the high pressure equilibrium cell, and then the equilibrium cell was closed. After the vacuum, the experiment was heated up to the set value and balance, and the CO_2 was injected. The CO_2 injection was stopped after the pressure and temperature of the system balanced. To simulate the conditions of deep coal in Zhengzhuang block, the experiments were conducted under various pressures and temperatures corresponding to the burial coal depths of 1000–2000 m (Table 2).

The volume analysis method was used to calculate the volume of CO_2 separated from the water solution according to the pressure in the equilibrium cell by gas state equation. Then the known concentration of NaOH solution was selected and the chemical titration was adopted to determine the amount of CO_2 in the remaining solution.

3.3. Evaluation Methods for CO_2 Storage Capacity

3.3.1. Adsorbed gas capacity

The dominance of single-layer sorption on coal results from its pore structure, where nearly 90% of all pores are ultramicropores (IUPAC), which have diameters similar to those of adsorbed gas particles (Pajdak et al., 2019). In most cases, the Langmuir model is used to solve the coal adsorption. However, under temperature and pressure conditions in deep coals, the D-R (Dubinin-Radushkevich) model may be a better solution to describe the gas sorption process (Sakurovs et al., 2007). Previous work has shown that the modified D-R model can be used to describe high pressure CO_2 sorption data when gas pressure is replaced with gas density (Sakurovs et al., 2007; Day et al., 2008a). For comparison, the D-R model was chosen to represent the excess sorption data for Zhengzhuang coal. The D-R model is given as follows (Day et al., 2008a):

$$n_{ex} = W_0(1-\rho_g/\rho_a)e^{-D[\ln(\rho_g/\rho_a)]^2} + k\rho_g, \quad (1)$$

where n_{ex} is the excess adsorption amount for the gas (cm^3/g), W_0 is the maximum sorption capacity of the coal (cm^3/g), ρ_g the density of the gas at the temperature and pressure (g/cm^3), ρ_a the density of the adsorbed phase (g/cm^3), D a constant which is a function of both the heat of adsorption and the affinity of the gas for the sorbent and k is a constant related to Henry's Law. In practice, k is strongly influenced by errors in cell volume and coal density and thus the value of k has high associated errors. The density of the adsorbed CO_2 phase, ρ_a, was taken to be 1.0 g/cm^3.

Based on the excess experimental data, also called the Gibbs excess adsorption, the absolute adsorption amount can be estimated by the equation given as (Pan and Connell, 2007):

$$n_{ab} = \frac{n_{ex}}{1-\rho_g/\rho_a} = \frac{n_{ex}}{1-P_eT_c/8ZP_cT_e}, \quad (2)$$

Table 2. Pressures and temperatures versus coal depth

Depth (m)	1000	1100	1200	1300	1400	1500	1600	1700	1800	1900	2000
Pressure (MPa)	9.7	10.72	11.74	12.76	13.78	14.8	15.82	16.84	17.86	18.88	19.9
Temperature (K)	317.55	321.05	324.55	328.15	331.65	335.15	338.75	342.25	345.75	349.25	352.85

where n_{ab} is the absolute adsorption amount for the gas (cm^3/g); P_c is the critical pressure of CO_2 (MPa), which takes the value of 7.383; T_c is the critical temperature of CO_2 (K), which takes the value of 304.21; P_e is the experimental pressure, and Z is the CO_2 compressibility factor (dimensionless). The values of the in situ CO_2 density and CO_2 compressibility factor were then estimated using the web-based Peace Software calculator (http://www.peacesoftware.de/einigewerte/cO2 e.html).

3.3.2. Free gas capacity

At very high pressures, the free gas content may become comparable to the adsorbed gas content (Saghafi, 2010; De Silva et al., 2012). However, the estimated free gas content of the seam was usually neglected. Therefore, the free gas content has to be included to increase the accuracy of the CO_2 storage capacity especially in its highly dense phase. According to the Mariotte's law, the free gas volume (n_f) that could be stored in coal seams could be found by using the following relationship:

$$n_f = \left(\frac{\varphi(1-S_w)}{\rho_{skeletal}\rho_b^{STP}} - V_a\right)\rho_g, \tag{3}$$

where n_f is the free gas content of coal, cm^3/g; φ is the porosity (fraction), %; S_w is the interconnected fracture water saturation (fraction), %; $\rho_{skeletal}$ is the apparent (skeletal) density of the coal, g/cm^3; ρ_b^{STP} is density of CO_2 in standard state, g/cm^3; V_a is sorbed-phase volume; ρ_g is the free gas density (g/cm^3), and could be calculated as:

$$\rho_g = \frac{M}{V_m} = \frac{PM}{ZRT}. \tag{4}$$

Assuming the sorbed-phase volume is negligible, and taking the volume away the free gas volume for the sorbed-phase is hard to calculate, and Equation (3) could be simplified to yield Equation (5):

$$n_f = \frac{\varphi(1-S_w)}{\rho_{skeletal}\rho_b^{STP}} \cdot \frac{PM}{ZRT}. \tag{5}$$

3.3.3. Soluble gas capacity

Having water is a significant characteristic in coal seams. The content of dissolved gas in the formation water is very low; however, for CO_2, it is not (Duan and Sun, 2003), and it is a function of pressure, temperature, etc. Dissolution of CO_2 into coal moisture may account for as much as 50% of the total sorption capacity for some low rank coals (Busch et al., 2007). So in this paper, the soluble gas content was considered. The gas dissolved in formation water in the coal seam could be given as follows:

$$n_s = \frac{\varphi S_w S_{CO_2}}{\rho_{skeletal}} \times 22.4, \tag{6}$$

where n_s is the soluble gas content (cm^3/g); S_{CO_2} is solubility of CO_2 in formation water (mol/cm^3), which can be determined experimentally.

4. RESULTS AND DISCUSSION

4.1. Effect of Depth on CO_2 Storage Capacity

4.1.1. Effect of depth on adsorbed gas content

The excess adsorption isotherms of A and B anthracite samples of Zhengzhuang coal are given (Fig. 3a). Both curves present the excess adsorption capacity, first increased, and then decreased with the increasing of adsorption equilibrium pressure. The excess adsorption capacity is decreased with the increasing temperature for the two samples. An obvious feature of the excess adsorption isotherm (especially A and B samples with a temperature of 353.15 K) presents a maximum value near the critical pressure point of CO_2 (7.38 MPa). The anomalous behaviors has been reported by some investigators with a highest pressure of 10 MPa

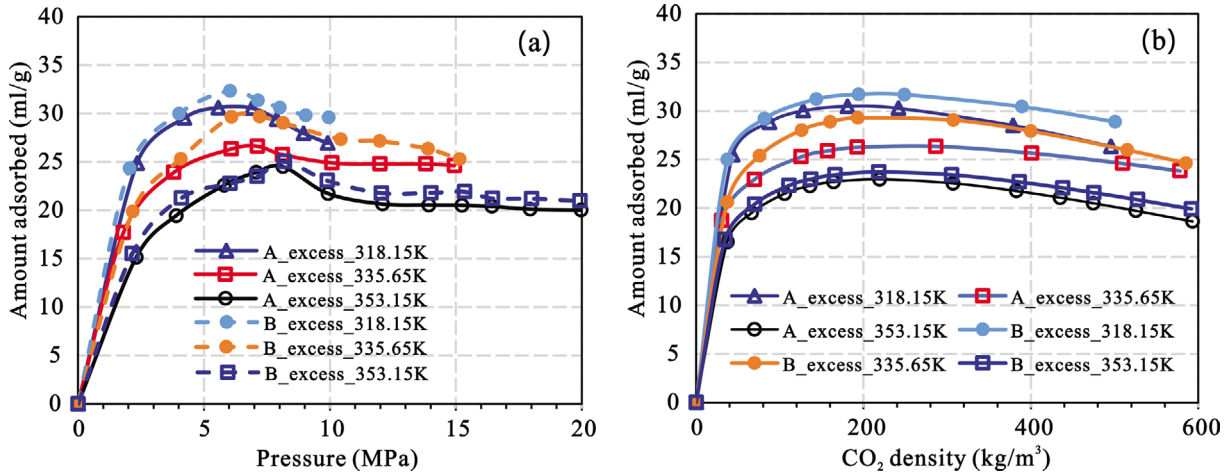

Fig. 3. CO_2 isotherms of A and B anthracite coals at different temperature as a function of pressure (a) and CO_2 density (b) showing the full range of sorption capacities.

https://doi.org/10.1007/s12303-020-0058-z

(Krooss et al., 2002; Siemons and Busch, 2007; Jinlong et al., 2018). It is also indicated that the classical Langmuir isotherm was not well suited for data fitting between the excess adsorption amount and adsorption equilibrium pressure.

Previous work has shown that a modified D-R model can be used to describe high pressure CO_2 sorption data when gas pressure is replaced with gas density (Sakurovs et al., 2007). Accordingly, the adsorbed data obtained in the Figure 3a were plotted as a function of CO_2 density through a fitting procedure proposed by the modified D-R model (Fig. 3b). All the shapes of the isotherms were similar, and excess adsorption reached a maximum at a gas density of between about 100 and 200 kg/m^3 after which sorption capacity decreased approximately rectilinearly. This decrease in excess adsorption is a result of the free gas density approaching that of the adsorbed phase (Jinlong et al., 2018). Measurements of CO_2 isotherms made in these experiments on several commercially available activated carbons have yielded an adsorbed phase density of 1000 kg/m^3 (Day et al., 2008b).

The absolute absorption isotherms of A and B anthracite samples are calculated (Fig. 4) by Equation (2) according to the corresponding excess adsorption isotherms. Obviously, the absolute adsorption capacity is increased with the increasing of the adsorption equilibrium pressure, which is obviously different with the excess adsorption isotherm. The absolute adsorption amounts of samples A and B are all over 44 cm^3/g at temperature 318.15, 335.65 and 353.15 K (Fig. 5). These values are larger than the excess adsorption amounts at the same temperatures. It is indicated that anthracite in deep coal seams in the study area may have a strong adsorption capacity of CO_2 under high pressure and temperature in deep coal seams.

The excess adsorption capacity initially increases indistinctively with the increase of depth in the 1000–1200 m range, passes through a maximum, and then decreases slightly up to 1500 m, then the trend is decreasing at depths of 1500–2000 m (Fig. 5). However, the absolute adsorption capacity shows an inverse trend by comparison. There are other significant differences between the observed excess adsorption quantity and the true absolute adsorption quantity (as determined by the D-R model) (Fig. 5). The absolute adsorption is 1.91–2.46 times larger or more than the excess adsorption under the same pressure. The difference between the amount of excess adsorption and absolute adsorption is increased with increasing depth, and the difference between them cannot be ignored, especially for coal seams over 1000 m deep. In order to obtain the accurate CO_2 storage capacity, the excess adsorbed capacity cannot be a part of the CO_2 storage capacity resulting in a large error in deep coals with both pressure and temperature effects.

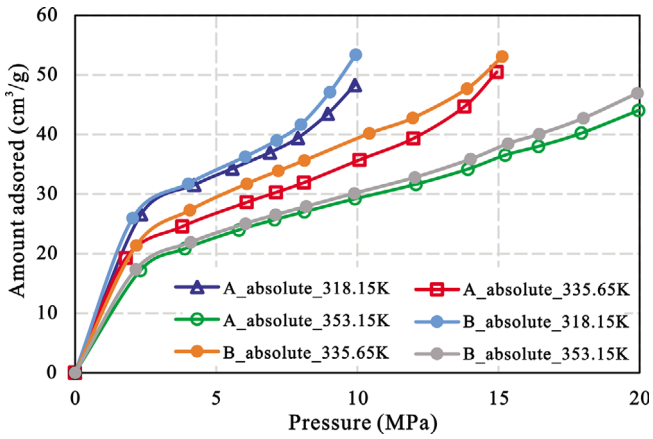

Fig. 4. CO_2 absolute isotherms of A and B anthracite coals at different temperature as a function of CO_2 pressure.

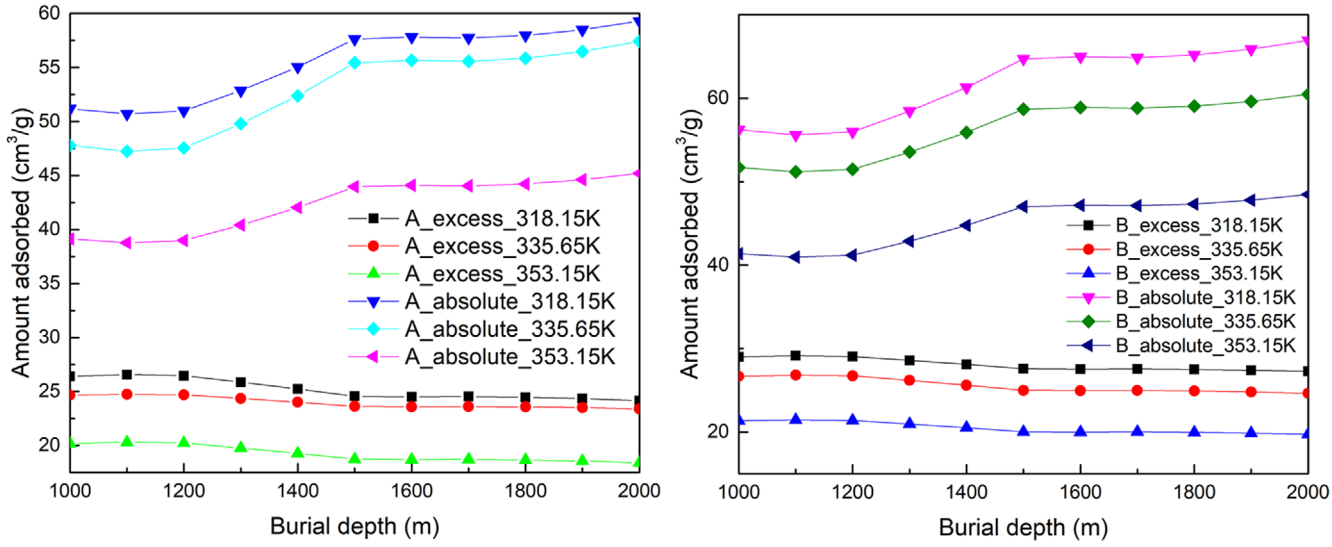

Fig. 5. Comparison of the excess adsorbed CO_2 content and absolute adsorbed CO_2 content under geological temperature and pressure conditions as they vary with depth.

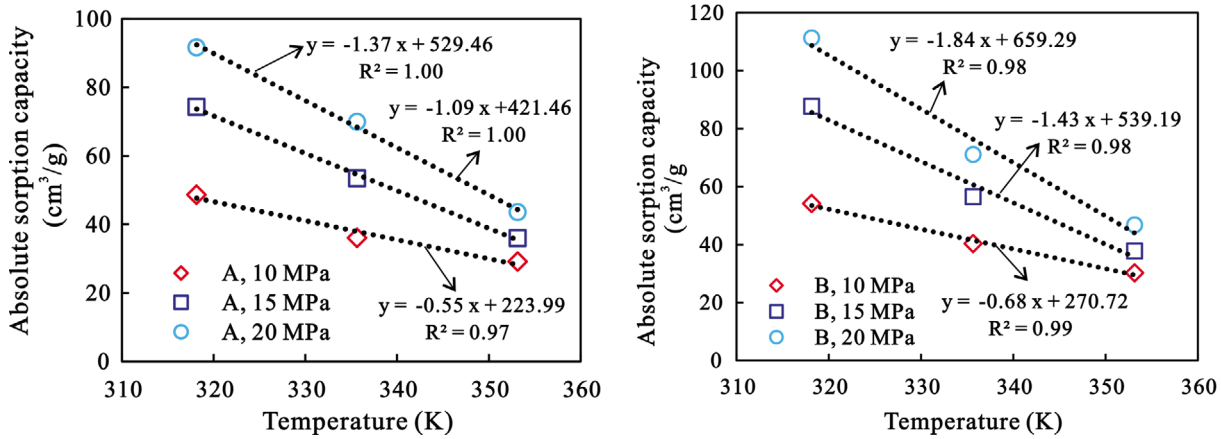

Fig. 6. CO_2 sorption for A and B anthracite coals as a function of temperature at different pressures.

As already mentioned above, it is shown here that gas sorption capacity decreases with temperature and this decrease is sharp with increased temperature, especially for pressures of 15 and 20 MPa used in the A and B coal samples (Fig. 6). The decrease in sorption capacity with temperature is about 0.39–1.50 cm^3/g per 1 K and 0.58–2.30 cm^3/g per 1 K for A and B samples, respectively. Regression for all linear fits is excellent with R^2 = 0.98–1.00.

4.1.2. Effect of depth on free gas content

According to Equation (5), substituting the in situ data such as coal reservoir temperature, pressure, and burial depth (Table 3) and parameters measured from simulated coal samples (Table 1), the free gas content of coals at different burial depths can be obtained (Fig. 7). It can be seen that the free gas content increases with increasing depth. Free gas molecules, together with adsorbed gas and moisture, fill the pore space in coal reservoir. Generally, free gas content has relations with factors of in situ porosity, initial water saturation and gas pressure in original position with increasing burial depth (Liu et al., 2013a). This section of the curves corresponds to depth less than 1400 m, in which the free gas content increases rapidly with the increasing burial depth. However, the free gas content curves slowly increase at the depth between 1400 m and 2000 m, and the increment of free gas content was small. These data indicated that the free gas content stored in anthracite in the study area have a relatively large percentage of total storage content, especially at the depths from 1400 to 2000 m.

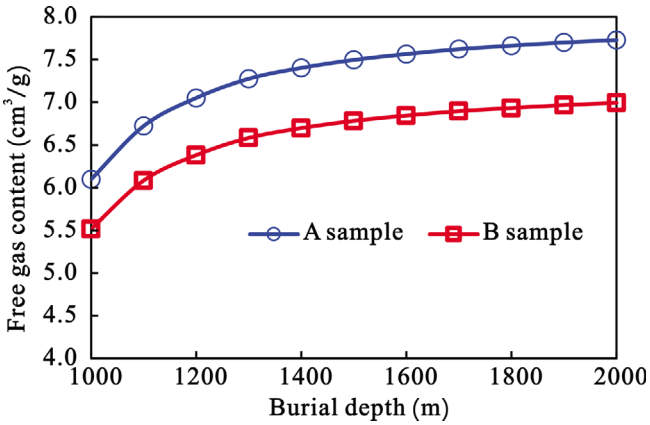

Fig. 7. Estimated free gas content at different depths.

4.1.3. Effect of depth on soluble gas content

According to test results of CO_2 solubility under simulated burial depths from 1000–2000 m, CO_2 solubility in each depth is acquired (Fig. 8a). The estimated CO_2 solubility is then used to determine the soluble gas content under the reservoir conditions. The CO_2 solubility tests, based on deionized purified water samples, present positive relationships with the changes of temperature and pressure, corresponding to a trend with the burial depth of

Table 3. CO_2 storage area divided according to calculated parameters

Area	Sub-area	Pressure (MPa)	Temperature (K)	Burial depth (m)	Permeability (mD)	RF	ER
Supercritical area	High-efficient storage area (I)	> 7.35	> 304.25	> 772	> 0.5	0.9	1.0
	Efficient storage area (II)	> 7.35	> 304.25	> 772	0.1–0.5	0.5	0.8
	Low-efficient storage area (III)	> 7.35	> 304.25	> 772	< 0.1	0.3	0.4
Subcritical area	Efficient storage area (IV)	< 7.35	< 304.25	< 772	0.1–0.5	0.5	0.8
	Low-efficient storage area (V)	< 7.35	< 304.25	< 772	< 0.1	0.3	0.4

RF – the recovery of coalbed methane, dimensionless; ER – the replacement coefficient, which is the ratio that CO_2 replace CH_4 in coal beds, dimensionless.

https://doi.org/10.1007/s12303-020-0058-z

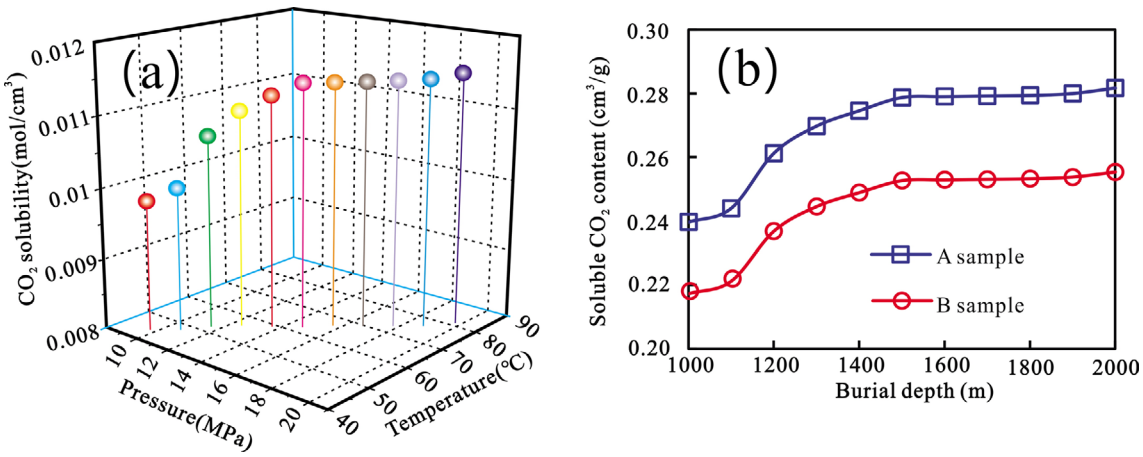

Fig. 8. The relationship between temperature, pressure and CO_2 solubility (a) and predicted soluble gas content at different burial depths (b) in the Zhengzhuang block.

1000–2000 m. According to the dissolution mechanism (Duan and Sun, 2003), the solubility for CO_2 depends on pressure and temperature. It increases with pressure and reduces with temperature. CO_2 solubility increases quickly with increasing depth less than 1500 m (about 15 MPa, 335.65 K), and exhibits a gently increasing trend when the depth is more than 1500 m. The results imply that the positive effect of pressure is larger than the negative effect of temperature under the conditions investigated. However, a negative effect of temperature is obvious below the depth of 1500–2000 m.

After converting the temperature and pressure into a function of depth (Eq. 6), the fitting trendline of obtained solubility with burial depth is shown below:

$$m_i = -3 \times 10^{-7} h^2 + 0.0011h + 0.208, \quad (7)$$

where m_i is the CO_2 solubility (mol/cm^3), $R^2 = 0.961$. This fitted equation was used to calculate the CO_2 solubility.

According to test results of CO_2 solubility under simulated depths (1000–2000 m), and considering the water saturation as a constant about 30%, soluble gas contents in No.3 coal seam at various burial depth are obtained and illustrated (Fig. 8b) by applying the coal reservoir conditions to the model (Eq. 6). However, the space that the water is displaced by CO_2 is not considered. At burial depths from 1000 m to 1300 m of the Zhengzhuang block, the soluble gas content of B sample varies from 0.22 cm^3/g to 0.24 cm^3/g (Fig. 8b). And then generally increases slowly from 1300 m to 2000 m, varying from 0.24 cm^3/g to 0.26 cm^3/g. Soluble gas content of A and B samples calculated by Equation (6) has an unobvious difference (about 0.02 cm^3/g) at the same depth because of their similar porosity and density, and constant water saturation of the two samples considered. Furthermore, the experiments of gas dissolving in water conducted by Liu et al. (2013a) revealed that the soluble gas in coals is also affected by temperature, pressure and salinity of coal seam water, etc.

4.2. Effect of Calculated Uncertainty on CO_2 Storage Capacity

There are many uncertainties associated with the considerations leading to CO_2 storage potential estimations in this study. Complex fault systems in the east study area (Fig. 1) may imply potential leakage pathways for injected CO_2 to the surface. However, currently there are no reliable approaches available for quantifying leakage through faults (Kronimus et al., 2008). Moreover, recent studies have shown that the CO_2 sorption capacity for various coals under the same experimental conditions can vary up to 100%, a potential error in the sorption capacity can be considered as high as 50% (Busch et al., 2003; Siemons and Busch, 2007; Kronimus et al., 2008). It's worth noting that a new technique for shale gas-in place calculations has been proposed (Ambrose et al., 2010), and thought that the volume of sorbed gas taken up must be determined and subtracted from the free gas calculation. Especially at high pressure, the volume occupied by the adsorbed phase may be increase because of the increasing adsorbed capacity of coal with increased pressure as mentioned in Figure 4.

Some other parameters were applied for this CO_2 storage, and these parameters could be obtained from different calculation models, experimental results or theoretical estimations. Therefore, there is a potential error in the CO_2 storage capacity estimation caused by the difference factors (Fig. 9).

The free gas content is affected obviously by CO_2 compressibility factor calculated by different methods (Fig. 9a) such as Benedict-Webb-Rubin-Starling state equation (BWRS), Soave-Redlich-Kwong state equation (SRK), Peng-Robinson state equation (PR) and Span-Wanger state equation (SW). These equations give variant CO_2 compressibility factors for the same depth with the same pressure and temperature. There is the largest variation of the free gas content with the aid of CO_2 compressibility factor

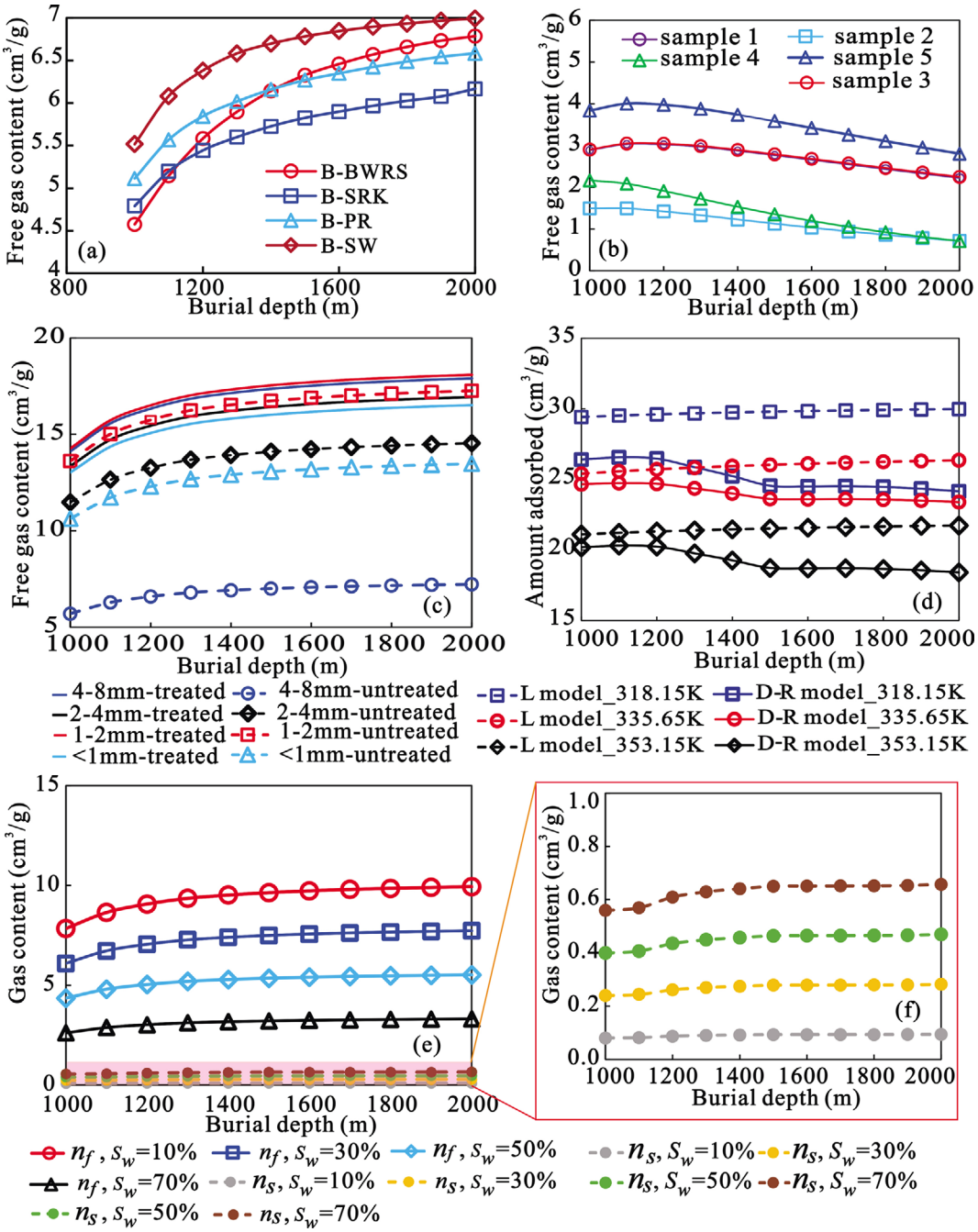

Fig. 9. Effect of Calculated uncertainty on CO_2 storage capacity induced by possible factors: (a) is an uncertainty of free CO_2 storage capacity caused by compressibility factor according to BWRS, SRK, PK and SW state equation; (b) is an uncertainty of free CO_2 storage capacity caused by porosity that decreases with the increasing of effective stress as a function of depth. The relationship between porosity and effective confining pressure was provided by Meng et al. (2015); (c) is an uncertainty of free CO_2 storage capacity caused by changing pore structure of coal before and after the supercritical CO_2 ($ScCO_2$) treatment with different coal grain sizes. The basic data of the untreated and $ScCO_2$-treated samples were given by Liu et al. (2010); (d) is two estimates of excess adsorbed CO_2 content considering a constant temperature with burial depth. L model: Langmuir model; D-R model: Dubinin-Radushkevich model; (e) is taking an example of A coal sample, which shows the results of free CO_2 storage capacity calculated by different water saturation in coal reservoir; (f) is enlarged in outset diagram of (e).

calculated by SW and SRK equation, respectively. The difference of the calculated free gas contents by the two methods can be up to 0.98 cm^3/g at the depth of 1300 m. In coal basins considered for Enhanced coal bed methane recovery (ECBM) production, the overburden stress increases with depth, and self-stressing of coal seams will occur due to swelling after CO_2 injection. Because of self-stressing of coal seams during CO_2-injection may be swelling associated with changed pore structure and CO_2 storage capacity (Hol et al., 2011). An uncertainty of free CO_2 storage capacity caused by porosity that decreases with the increasing of

https://doi.org/10.1007/s12303-020-0058-z

effective stress as a function of depth (Fig. 9b). Porosity data indicate a higher effective stress corresponds to a lower porosity, which may cause a decrease of free gas content as the burial increases with a decreasing porosity. Changing porosities with the same burial depth demonstrates the relationship of porosity and burial depth as well as related function should be considered for CO_2 storage calculation.

Moreover, pore structure changes in coal during the CO_2 geo-sequestration is one of the key issues that affect the sequestration process significantly (Liu et al., 2010). During the process of CO_2 sequestration, CO_2 is distributed into the coal reservoir through the coal cleat system and then stored within the coal matrix (Massarotto et al., 2010) due to the strong affinity between CO_2 and coal substance. A consequence is that the pore structure and pore size distribution of coal may be significantly changed, which in turn affects the sequestration process and hence the performance of CO_2 storage in coal seams. The free gas content comparison of samples with and without $ScCO_2$-H_2O treatment of different grain size are compared (Fig. 9c). These similar curves show a larger difference of free gas content between treated or untreated samples. Taking treated/untreated 2–4 mm grain size samples for example, the increment of the free gas content is 1.89 cm^3/g corresponding the porosity changing from 7.41% (untreated sample) to 12.37% (treated sample). Therefore, an additional estimated error may be possible if the pore structure parameters of the $ScCO_2$ untreated sample were used for CO_2 storage estimation. Hence, the estimation of CO_2 storage capacity, which represents the ultimate storage limit, should be more accurate according to some experimental parameters obtained by the $ScCO_2$ treated sample.

It is not surprising that many adsorption models have been used to estimate the coal adsorption capacity, such as Langmuir model, D-R model and so on. However, these models have different applied mechanisms for different types of coals and conditions such as highly dense phase CO_2 conditions. The Langmuir model is widely used to estimate the pure gas adsorption capacity or monolayer adsorption capacity. As previously mentioned, the Langmuir model is presented as a possible solution at supercritical conditions. Therefore, the Langmuir model is chosen here to compare with the D-R model used in this study, which can demonstrate that an optimized adsorption model is needed to accurately describe the adsorption behavior of CO_2 storage estimation in coal. There are significant differences between two estimates of excess adsorbed CO_2 content (Fig. 9d). The oversimplified prediction of excess adsorption by Langmuir model is 1.03–1.24 times larger or more than the data estimated by the D-R model. With increasing burial depth, the difference values generally decreased and then increased at three given temperatures. Using the Langmuir model at temperature 318.15, 335.65, and 353.15 K the adsorbed CO_2 storage capacity at a depth of 1000 m are overestimated (11%, 3% and 5%), and at a depth of 2000 m are overestimated (24%, 13% and 18%), respectively. To determine accurately the CO_2 storage capacity, one must employ an accurate adsorption model. If either an oversimplified adsorbed model or the measured excess adsorption quantity is used, the result will be a significant over-estimation of contribution to the total storage capacity from adsorbed CO_2 under real geological conditions.

Further, the water can be displaced by CO_2 during the process of CO_2 sequestration, and this process provides additional space for free CO_2 storage but decreases dissolved CO_2 in the residual water because of remaining water saturation. By utilizing an assumption of the water and gas saturation, the free gas and soluble gas content are shown, respectively (Figs. 9e and f). It can be seem that the increase of water saturation causes an increase of dissolved gas but a decrease of free gas. If the same coal seam at the end of CO_2 injection has high gas saturation and low water saturation, it will inevitably lead to higher free gas content and lower water soluble gas content, and vice versa.

There are also some other uncertainties associated with the considerations leading to CO_2 storage potential estimations in this study. Complex fault systems in the east study area (Fig. 1) may imply potential leakage pathways for injected CO_2 to the surface. However, currently there are no reliable approaches available for quantifying leakage through faults (Kronimus et al., 2008). Moreover, recent studies have shown that the CO_2 sorption capacity for various coals under the same experimental conditions can vary up to 100%, a potential uncertainty in the sorption capacity can be considered as high as 50% (Busch et al., 2003; Siemons and Busch, 2007; Kronimus et al., 2008). It's worth noting that the estimation of CO_2 storage capacity in coal seam is a complex process with highly uncertain because it depends on the distributions of coal thickness, coal quality, gas content, gas saturation, estimation method, etc. A successful CO_2 storage capacity estimation has to account for adsorbed gas content, free gas content and soluble gas content with important geological and reservoir parameters (coal quality, pressure, temperature, porosity, permeability, etc.) to estimate the CO_2 gas content potential. Hence, improved field data, laboratory data and appropriate evaluation methods can improve the accuracy of the estimation result.

4.3. Total CO_2 Storage Capacity in Study Area

The CO_2 storage in coal seams with water should consider three factors: a sorbed phase consisting of gas molecules adhering to the surface of the coal matrix, n_{ab} (cm^3/g), which is the absolute amount of adsorbed gas; free gas within the pores and natural

fractures, n_f (cm^3/g); and gas dissolved in formation water in the coal seam (n_s, cm^3/g). Hence, we have M_{co_2} as the total gas in place:

$$M_{co_2} = \rho_g \times A \times H \times \rho_{bulk} \times (n_f + n_s + n_{ab}), \quad (8)$$

where M_{co_2} is the total storage gas in coal seam, t; A is the area of coal beds basin, m^2; H is the thickness of coal beds, m; ρ_{bulk} is the bulk coal density (g/cm^3); n_{ab} is generally assumed to follow a D-R isotherm in theses A and B coal samples (from Eqs. 1 and 2). The free gas content (n_f) and soluble gas capacity can be calculated by Equations (5) and (6), respectively. This capacity represents the ultimate storage limit that could be attained.

According to the relation of temperature, pressure, and burial depth, the research area can be divided into a supercritical area of CO_2 storage and a sub-critical area of CO_2 storage (Table 3). Moreover, the permeability distribution of No.3 coal seam was drawn by superimposing the contour map of coal structure, joint density, and measured fracture development. Therefore, sub-areas of CO_2 storage were divided (Table 3). Selective replacement coefficient and recovery can be assumed because of the impact of permeability on effective storage capacity (Table 3). All parameters (Table 4) used for this calculation are listed. The measured reservoir pressure of coal at different depths were used to estimate the pressure which changes with the depth of the coal bed by linear fitting method (Yang et al., 2018; Liu et al., 2019a; Du et al., 2020). According to the uncertainty analysis, the best parameters are determined for storage capacity estimation according to their variation with coal burial depth. The pressures and temperatures, reaching more than 7.38 MPa (critical pressure) and 304.25 K (critical temperature), respectively, are passed from east to west through the central of the study area (blue dotted line (Fig. 10), representing a boundary of CO_2 phase change). The range from the boundary of CO_2 phase change to the north boundary provides a target area for the $ScCO_2$ storage. A summary of the results (Table 5) is presented. The largest total storage capacity is over 6.65×10^8 t, and the effective storage capacity is only 1.48×10^8 t based on additional replacement coefficient and recovery in the identified storage of 713 km^2. The effective storage capacity is only 1.21×10^8 t in the supercritical area, while the high-efficient area is only 5.52×10^6t. Supercritical storage capacity is nearly 3.5 times as large as sub-critical storage capacity, although the two areas are nearly equal. Most of the storage CO_2 is adsorptive, and soluble content accounted for less than 1.0% and free gas nearly up to 14%, which suggested that the soluble gas content can be ignored in the process of storage capacity estimation, but free gas content has a relatively large proportion in total storage content. The assumed replacement and recovery factors, while realistic, are somewhat arbitrary and on the optimistic side (Bachu, 2007; Kronimus et al., 2008). As experience is gained with CO_2 storage operations, these parameters can be easily modified and applied anew to improve the capacity estimates and identify the coal seam with the highest potential.

Table 4. A summary of parameters used for determination of potential CO_2 storage

Parameter	Remarks
Pressure and temperature	$P = 0.0102h - 0.4959$, $T_f = 0.0353h + 555.37$ (Yang et al., 2018; Liu et al., 2019a; Du et al., 2020)
Coal density and porosity	Illustrated by Table 1, sample A with Hg intrusion method.
CO_2 compressibility factor and density	Estimated using the web-based Peace Software calculator (http://www.peacesoftware.de/einigewerte/cO$_2$ e.html).
Adsorption gas content model	Illustrated by Equations (1) and (2), determination of sorption parameters at 318.15 K of sample A.
Free gas content model and soluble gas content model	Illustrated by Equations (5) and (6), respectively.
Total limited CO_2 storage capacity model	Illustrated by Equation (8).
Water saturation	Assumed 30% based on statistic data of coalbed methane.

Note: h, coal depth, m; P, coal reservoir pressure, MPa; T_f, coal reservoir temperature, K.

Table 5. The evaluation results for CO_2 storage capacity in Zhengzhuang block of South Qinshui Basin

Sub-area	I	II	III	IV	V
Adsorption storage (t)	5.25×10^6	1.69×10^8	2.72×10^8	3.13×10^7	1.05×10^8
Dissolution storage (t)	3.33×10^4	1.05×10^6	1.78×10^6	1.75×10^5	6.00×10^5
Free storage (t)	8.46×10^5	2.34×10^7	4.35×10^7	2.72×10^6	8.31×10^6
Total storage capacity (t)	6.13×10^6	1.94×10^8	3.17×10^8	3.42×10^7	1.14×10^8
Effective storage capacity (t)	5.52×10^6	7.74×10^7	3.80×10^7	1.37×10^7	1.37×10^7
Percentage of free CO_2 (%)	13.8	12.1	13.72	7.96	7.31
Percentage of soluble CO_2 (%)	0.54	0.54	0.56	0.51	0.53
Percentage of adsorbed CO_2 (%)	85.66	87.35	85.72	91.52	92.16

https://doi.org/10.1007/s12303-020-0058-z

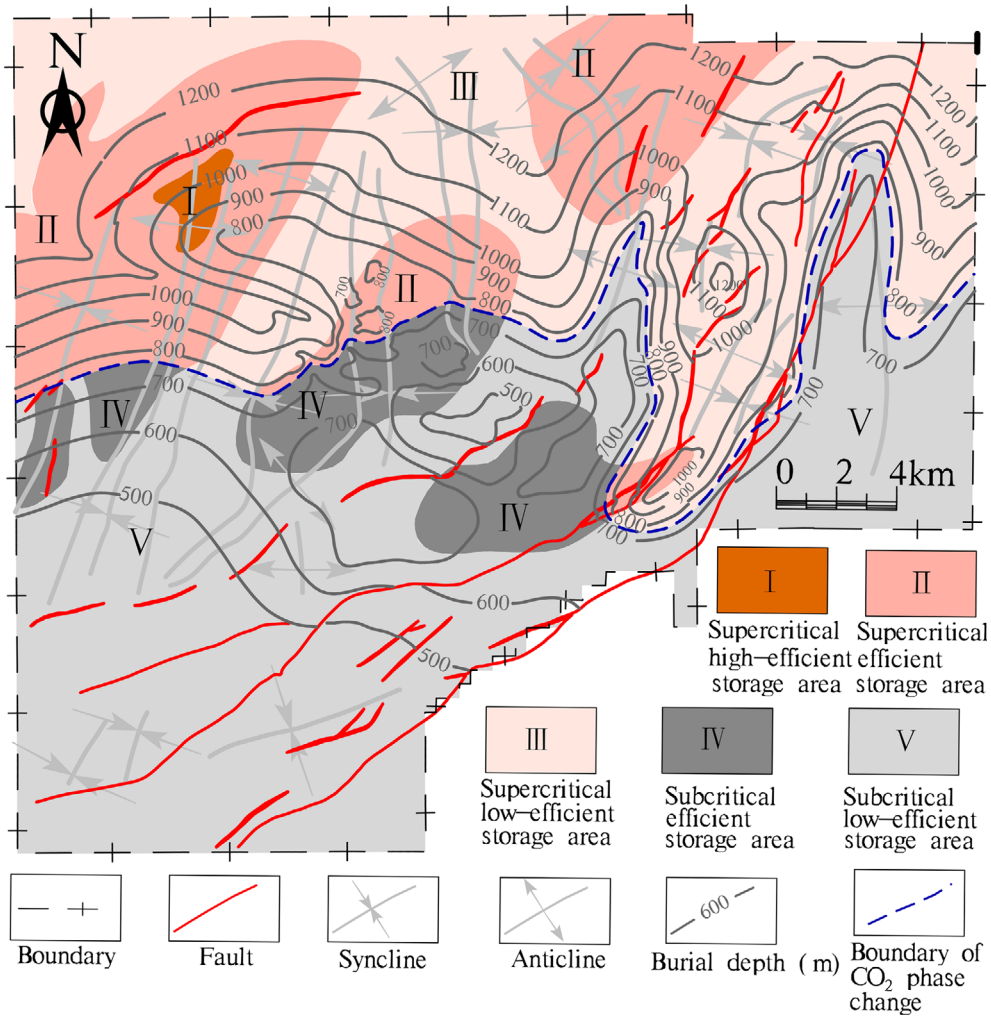

Fig. 10. Burial depth and thickness of No. 3 coal seam in Zhengzhuang block (Units of contour lines: m for burial depth of coal seam No. 3 and m for coal seam thickness with contour lines).

5. CONCLUSIONS

(1) The selected anthracites of the No. 3 coal seam in Qinshui basin of China were tested at reservoir temperatures and pressures to provide important information of which are vital for prediction of CO_2 storage capacity in coal seams. The evaluation method considered desorbed gas, free gas and soluble gas to improve the accuracy of CO_2 storage evaluation results.

(2) The adsorbed and free gas content of the anthracites are 35–70 cm^3/g and 5–8 cm^3/g, respectively within a varying depth of 1000–2000 m in the study area, and the soluble gas can be ignored because of its low content between 0.22 cm^3/g and 0.28 cm^3/g with a proportion of less than 1%. The study area was divided into five sub-areas to estimate the CO_2 storage capacity. Supercritical storage capacity is nearly 3.5 times as large as sub-critical storage capacity, although the two areas are nearly equal.

(3) Some uncertainties about coal reservoir, such as porosity, water saturation, geological structure, and adsorption model represent possible changes in actual geological conditions to estimate the CO_2 storage capacity. Uncertainties related to storage capacity estimation can be minimized by improving field data, laboratory data and appropriate evaluation methods.

ACKNOWLEDGMENTS

This work was supported by the Natural Science Research Project of Anhui Universities (KJ2020A0317), the National Natural Science Foundation of China (Grant No. 41727801, 41330638), the Key Research and Development Program of Anhui Province (Grant No. 1804a0802203), Program of Study Abroad for Young Scholar sponsored by Education Department of Anhui Province (gxgwfx2019012), the University Natural Science Research Project of Anhui Province (KJ2019A0100) and the National Science Foundation of Anhui Province (2008085MD121).

REFERENCES

Ambrose, R.J., Hartman, R.C., Diaz Campos, M., Akkutlu, I.Y., and Sondergeld, C., 2010, New pore-scale considerations for shale gas in place calculations. Proceedings of the SPE Unconventional Gas Conference, Pittsburgh, Feb. 23–25, p. 17.

Ampomah, W., Balch, R., Will, R., Cather, M., Gunda, D., and Dai, Z., 2017, Co-optimization of CO_2-EOR and storage processes under geological uncertainty. Energy Procedia, 114, 6928–6941.

Bachu, S., 2007, Carbon dioxide storage capacity in uneconomic coal beds in Alberta, Canada: Methodology, potential and site identification. International Journal of Greenhouse Gas Control, 1, 374–385.

Bachu, S., Bonijoly, D., Bradshaw, J., Burruss, R., Holloway, S., Christensen, N.P., and Mathiassen, O.M., 2007, CO_2 storage capacity estimation: Methodology and gaps. International Journal of Greenhouse Gas Control, 1, 430–443.

Bae, J.S. and Bhatia, S.K., 2006, High-pressure adsorption of methane and carbon dioxide on coal. Energy & Fuels, 20, 2599–2607.

Busch, A. and Gensterblum, Y., 2011, CBM and CO_2-ECBM related sorption processes in coal: a review. International Journal of Coal Geology, 87, 49–71.

Busch, A., Gensterblum, Y., and Krooss, B.M., 2003, Methane and CO_2 sorption and desorption measurements on dry Argonne premium coals: pure components and mixtures. International Journal of Coal Geology, 55, 205–224.

Busch, A., Gensterblum, Y., and Krooss, B.M., 2007, High-pressure sorption of nitrogen, carbon dioxide, and their mixtures on argonne premium coals. Energy & Fuels, 21, 1640–1645.

Cai, Y., Liu, D., Yao, Y., Li, J., and Qiu, Y., 2011, Geological controls on prediction of coalbed methane of No. 3 coal seam in Southern Qinshui Basin, North China. International Journal of Coal Geology, 88, 101–112.

Chen, B., Harp, D.R., Lu, Z., and Pawar, R.J., 2020, Reducing uncertainty in geologic CO_2 sequestration risk assessment by assimilating monitoring data. International Journal of Greenhouse Gas Control, 94, 102926.

Chen, S., Tang, D., Tao, S., Xu, H., Li, S., Zhao, J., Cui, Y., and Li, Z., 2018, Characteristics of in-situ stress distribution and its significance on the coalbed methane (CBM) development in Fanzhuang-Zhengzhuang Block, Southern Qinshui Basin, China. Journal of Petroleum Science and Engineering, 161, 108–120.

Day, S., Duffy, G., Sakurovs, R., and Weir, S., 2008a, Effect of coal properties on CO_2 sorption capacity under supercritical conditions. International Journal of Greenhouse Gas Control, 2, 342–352.

Day, S., Sakurovs, R., and Weir, S., 2008b, Supercritical gas sorption on moist coals. International Journal of Coal Geology, 74, 203–214.

De Silva, P.N.K. and Ranjith, P.G., 2014, Understanding and application of CO_2 adsorption capacity estimation models for coal types. Fuel, 121, 250–259.

De Silva, P.N.K., Ranjith, P.G., and Choi, S.K., 2012, A study of methodologies for CO_2 storage capacity estimation of coal. Fuel, 91, 1–15.

Du, Y., Fu, C., Pan, Z., Sang, S., Wang, W., Liu, S., Zhao, Y., and Zhang, J., 2020, Geochemistry effects of supercritical CO_2 and H_2O on the mesopore and macropore structures of high-rank coal from the Qinshui Basin, China. International Journal of Coal Geology, 223, 103467.

Duan, Z. and Sun, R., 2003, An improved model calculating CO_2 solubility in pure water and aqueous NaCl solutions from 273 to 533 K and from 0 to 2000 bar. Chemical Geology, 193, 257–271.

Fang, H., Sang, S., Liu, S., and Liu, S., 2019, Experimental simulation of replacing and displacing CH_4 by injecting supercritical CO_2 and its geological significance. International Journal of Greenhouse Gas Control, 81, 115–125.

Gale, J., Abanades, J.C., Bachu, S., and Jenkins, C., 2015, Special issue commemorating the 10th year anniversary of the publication of the Intergovernmental panel on climate change special report on CO_2 capture and storage. International Journal of Greenhouse Gas Control, 40, 1–5.

Gale, J.J. and Freund, P., 2010, Coal-bed methane enhancement with CO_2 sequestration worldwide potential. Environmental Geosciences, 8, 210–217.

Chinese National Standard GB/T 212-2008, 2008, Proximate analysis of coal. Certification and Accreditation Administration of the People's Republic of China, Beijing.

Chinese National Standard GB/T 19560-2008, 2008, Experimental method of high-pressure isothermal adsorption to coal. Certification and Accreditation Administration of the People's Republic of China, Beijing.

Chinese National Standard GB/T 21650-2008, 2008, Pore size distribution and porosity of solid materials by mercury porosimetry and gas adsorption. Certification and Accreditation Administration of the People's Republic of China, Beijing.

Chinese National Standard GB/T 8899-2013, 2013, Determination of maceral group composition and minerals in coal. Certification and Accreditation Administration of the People's Republic of China, Beijing.

Hol, S., Peach, C.J., and Spiers, C.J., 2011, Applied stress reduces the CO_2 sorption capacity of coal. International Journal of Coal Geology, 85, 128–142.

Höller, S. and Viebahn, P., 2016, Facing the uncertainty of CO_2 storage capacity in China by developing different storage scenarios. Energy Policy, 89, 64–73.

Jinlong, J., Shuxun, S., Liwen, C., and Shiqi, L., 2018, Characteristics of CO_2/supercritical CO_2 adsorption-induced swelling to anthracite: an experimental study. Fuel, 216, 639–647.

Kim, H.J., Shi, Y., He, J., Lee, H.-H., and Lee, C.-H., 2011, Adsorption characteristics of CO_2 and CH_4 on dry and wet coal from subcritical to supercritical conditions. Chemical Engineering Journal, 171, 45–53.

Kronimus, A., Busch, A., Alles, S., Juch, D., Jurisch, A., and Littke, R., 2008, A preliminary evaluation of the CO_2 storage potential in unminable coal seams of the Münster Cretaceous Basin, Germany. International Journal of Greenhouse Gas Control, 2, 329–341.

Krooss, B.M., van Bergen, F., Gensterblum, Y., Siemons, N., Pagnier, H.J.M., and David, P., 2002, High-pressure methane and carbon dioxide adsorption on dry and moisture-equilibrated Pennsylvanian coals. International Journal of Coal Geology, 51, 69–92.

Li, D., Liu, Q., Weniger, P., Gensterblum, Y., Busch, A., and Krooss, B.M., 2010, High-pressure sorption isotherms and sorption kinet-

https://doi.org/10.1007/s12303-020-0058-z

ics of CH_4 and CO_2 on coals. Fuel, 89, 569–580.

Liu, A., Fu, X., Wang, K., An, H., and Wang, G., 2013a, Investigation of coalbed methane potential in low-rank coal reservoirs – free and soluble gas contents. Fuel, 112, 14–22.

Liu, C., Sang, S., Fan, X., Zhang, K., Song, F., Cui, X., and Wang, H., 2020a, Influences of pressures and temperatures on pore structures of different rank coals during CO_2 geological storage process. Fuel, 259, 116273.

Liu, C., Sang, S., Zhang, K., Song, F., Wang, H., and Fan, X., 2019a, Effects of temperature and pressure on pore morphology of different rank coals: implications for CO_2 geological storage. Journal of CO_2 Utilization, 34, 343–352.

Liu, C.J., Wang, G.X., Sang, S.X., and Rudolph, V., 2010, Changes in pore structure of anthracite coal associated with CO_2 sequestration process. Fuel, 89, 2665–2672.

Liu, H., Sang, S., Formolo, M., Li, M., Liu, S., Xu, H., An, S., Li, J., and Wang, X., 2013b, Production characteristics and drainage optimization of coalbed methane wells: a case study from low-permeability anthracite hosted reservoirs in southern Qinshui Basin, China. Energy for Sustainable Development, 17, 412–423.

Liu, H., Sang, S., Wang, G.G.X., Li, M., Xu, H., Liu, S., Li, J., Ren, B., Zhao, Z., and Xie, Y., 2014, Block scale investigation on gas content of coalbed methane reservoirs in southern Qinshui basin with statistical model and visual map. Journal of Petroleum Science and Engineering, 114, 1–14.

Liu, H.H., Sang, S.X., Liu, S.M., Wu, H.Y., Lan, T.H., Xu, H.J., and Ren, B., 2019b, Supercritical-CO_2 adsorption quantification and modeling for a deep coalbed methane reservoir in the Southern Qinshui Basin, China. ACS Omega, 4, 11685–11700.

Liu, S., Fang, H., Sang, S., Ashutosh, T., Wu, J., Zhang, S., and Zhang, B., 2020b, CO_2 injectability and CH_4 recovery of the engineering test in qinshui Basin, China based on numerical simulation. International Journal of Greenhouse Gas Control, 95, 102980.

Liu, S., Ma, J., Sang, S., Wang, T., Du, Y., and Fang, H., 2018, The effects of supercritical CO_2 on mesopore and macropore structure in bituminous and anthracite coal. Fuel, 223, 32–43.

Liu, S., Sang, S., Ma, J., Wang, T., Du, Y., and Fang, H., 2019c, Effects of supercritical CO_2 on micropores in bituminous and anthracite coal. Fuel, 242, 96–108.

Liu, Y.F., Xiao-Chun, L.I., and Bing, B., 2005, Preliminary estimation of CO_2 storage capacity of coalbeds in China. Chinese Journal of Rock Mechanics & Engineering, 24, 2947–2952.

Massarotto, P., Golding, S.D., Bae, J.S., Iyer, R., and Rudolph, V., 2010, Changes in reservoir properties from injection of supercritical CO_2 into coal seams – a laboratory study. International Journal of Coal Geology, 82, 269–279.

Meng, Y., Li, Z., and Lai, F., 2015, Experimental study on porosity and permeability of anthracite coal under different stresses. Journal of Petroleum Science and Engineering, 133, 810–817.

Pajdak, A., Skoczylas, N., Dębski, A., Grzegorek, J., Maziarz, W., and Kudasik, M., 2019, CO_2 and CH_4 sorption on carbon nanomaterials and coals – comparative characteristics. Journal of Natural Gas Science and Engineering, 72, 103003.

Pan, Z. and Connell, L.D., 2007, A theoretical model for gas adsorption-induced coal swelling. International Journal of Coal Geology, 69, 243–252.

Pan, Z., Connell, L., Shangzhi, M., Sander, R., Camilleri, M., Down, D.I., Carras, J., Lu, M., Xiaokang, F., Wenzhong, Z., Benguang, G., Jianping, Y., Briggs, C., and Lupton, N., 2013, CO_2 injectivity in a multi-lateral horizontal well in a low permeability coal seam: results from a field trial. Energy Procedia, 37, 5834–5841.

Ramasamy, S., Sripada, P.P., Khan, M.M., Tian, S., Trivedi, J., and Gupta, R., 2014, Adsorption behavior of CO_2 in coal and coal char. Energy & Fuels, 28, 5241–5251.

Saghafi, A., 2010, Potential for ECBM and CO_2 storage in mixed gas Australian coals. International Journal of Coal Geology, 82, 240–251.

Sakurovs, R., Day, S., and Weir, S., 2009, Causes and consequences of errors in determining sorption capacity of coals for carbon dioxide at high pressure. International Journal of Coal Geology, 77, 16–22.

Sakurovs, R., Day, S., Weir, S., and Duffy, G., 2007, Application of a modified Dubinin-Radushkevich equation to adsorption of gases by coals under supercritical conditions. Energy & Fuels, 21, 992–997.

Siemons, N. and Busch, A., 2007, Measurement and interpretation of supercritical CO_2 sorption on various coals. International Journal of Coal Geology, 69, 229–242.

Su, X., Lin, X., Liu, S., Zhao, M., and Song, Y., 2005, Geology of coalbed methane reservoirs in the Southeast Qinshui Basin of China. International Journal of Coal Geology, 62, 197–210.

Tayari, F. and Blumsack, S., 2020, A real options approach to production and injection timing under uncertainty for CO_2 sequestration in depleted shale gas reservoirs. Applied Energy, 263, 114491.

Wen, S., Zhou, K., and Lu, Q., 2019, A discussion on CBM development strategies in China: a case study of PetroChina Coalbed Methane Co., Ltd. Natural Gas Industry B, 6, 610–618.

Xu, H., Pan, Z., Hu, B., Liu, H., and Sun, G., 2020, A new approach to estimating coal gas content for deep core sample. Fuel, 277, 118246.

Xu, H., Sang, S., Yang, J., Jin, J., Liu, H., Zhou, X., and Gao, W., 2019, Evaluation of coal and shale reservoir in Permian coal-bearing strata for development potential: a case study from well LC-1# in the northern Guizhou, China. Energy Exploration & Exploitation, 37, 194–218.

Yang, J., Xu, H., Liu, H., Ouyang, X., and Han, S., 2018, Theoretical storage capacity of free carbon dioxide and its influence factors of anthracite in Jincheng. Coal Geology & Exploration, 46, 49–54.

Zhang, J., Liu, K., Clennell, M.B., Dewhurst, D.N., and Pervukhina, M., 2015, Molecular simulation of CO_2-CH_4 competitive adsorption and induced coal swelling. Fuel, 160, 309–317.

Zhao, X., Liao, X., and He, L., 2016, The evaluation methods for CO_2 storage in coal beds, in China. Journal of the Energy Institute, 89, 389–399.

APPENDIX

A : Area of coal beds basin, m^2
A_{ad} : Ash content of air-dried basis
BWRS : Benedict-Webb-Rubin-Starling state equation
C_{daf} : Carbon content of dry ash-free basis
CBM : Coalbed methane
D : Constant which is a function of both the heat of adsorption and the affinity of the gas for the sorbent and
D-R model : Dubinin-Radushkevich model
ECBM : Enhanced coal bed methane recovery
ER : Replacement coefficient, which is the ratio that CO_2 replace CH_4 in coal beds, dimensionless
Exi : Exinite
F_{Cad} : Fixed carbon carbon content of air-dried basis
h : Coal depth, m
H : Thickness of coal beds, m
H_{daf} : Hydrogen content of dry ash-free basis
Iip : Liptinite
IUPAC : International union of pure and applied chemistry
k : Constant related to Henry's Law
M_{ad} : Moisture content of air-dried basis
M_{co_2} : Total storage gas in coal seam, t
m_i : CO_2 solubility, mol/cm^3
Min : Mineral
n_{ab} : Absolute adsorption amount for the gas, cm^3/g
n_{ex} : Excess adsorption amount for the gas, cm^3/g
N_{daf} : Nitrogen content of dry ash-free basis
n_f : Free gas content of coal, cm^3/g
n_s : Soluble gas content, cm^3/g
O_{daf} : Oxygen content of dry ash-free basis
P : Coal reservoir pressure, MPa
P_c : Critical pressure of CO_2 (MPa), which takes the value of 7.383
P_e : Experimental pressure
PR : Peng-Robinson state equation
R : 8.31 J/(mol·K)
RF : Recovery of coalbed methane, dimensionless
S_{co_2} : Solubility of CO_2 in formation water (mol/cm^3), which can be determined experimentally
S_{daf} : Sulphur content of dry ash-free basis
S_w : Interconnected fracture water saturation (fraction), %
SRK : Soave-Redlich-Kwong state equation
T : Thermodynamic temperature, K
T_c : Critical temperature of CO_2 (K), which takes the value of 304.21
T_f : Coal reservoir temperature, K
SW : Span-Wanger state equation
V_a : Dorbed-phase volume
V_{daf} : Volatile content of dry ash-free basis
Vit : Vitrinite
W_0 : Maximum sorption capacity of the coal, cm^3/g
Z : CO_2 compressibility factor (dimensionless)
ρ_a : Density of the adsorbed phase, g/cm^3
ρ_{bulk} : Bulk density, g/cm^3
ρ_b^{STP} : Density of CO_2 in standard state, g/cm^3
ρ_g : Free gas density, g/cm^3
$\rho_{skeletal}$: Apparent (skeletal) density, g/cm^3
φ : Porosity (fraction), %

https://doi.org/10.1007/s12303-020-0058-z